The ameliorative effect of terpinen-4-ol on ER stress-induced vascular calcification depends on sirt1-mediated regulation of PERK acetylation

Yan-Yan Zhang
Guizhou Medical University
Li He
Guizhou Medical University
Meng-Xin Tu
Guizhou Medical University
Mei Huang
Guizhou Medical University
Yan Chen
Guizhou Medical University
Di Pan
Guizhou Medical University
Jian-Qing Peng
Guizhou Medical University
Xiangchun Shen (shenxiangchun@126.com)
Guizhou Medical University https://orcid.org/0000-0002-4390-0725

Original investigation

Keywords: Vascular calcification, terpinen-4-ol, sirt1, ER stress, PERK acetylation

Posted Date: January 29th, 2021

DOI: https://doi.org/10.21203/rs.3.rs-154937/v1

Abstract

Background

Endoplasmic reticulum (ER) stress-mediated phenotypic switching of vascular smooth muscle cells (VSMCs) is key to vascular calcification (VC) in patients with chronic kidney disease (CKD). Terpinen-4-ol exerts protective effect against cardiovascular disease, but its role and specific mechanism in VC remain unclear. We explored whether terpinen-4-ol alleviates ER stress-mediated VC through sirtuin 1 (sirt1) and elucidated its mechanism to provide evidence for its application in the clinical prevention and treatment of VC.

Methods

In this study, CKD-related VC animal model and β-glycerophosphate (β-GP)-induced VSMCs calcification model were established. We investigated the part of terpinen-4-ol in ER stress-induced VC *in vitro and in vivo*. However, in order to clarify whether terpinen-4-ol inhibits the molecular mechanism of ERs-induced VC through sirt1, we further verified the above signal transduction by knocking down sirt1 *in vitro and in vivo*.

Results

Terpinen-4-ol inhibited calcium deposition, phenotypic switching, and ER stress of VSMCs *in vitro* and *in vivo*. Furthermore, pre-incubation with terpinen-4-ol or a sirt1 agonist and transfection with lentivirus overexpressing sirt1 decreased β-GP-induced calcium salt deposition, increased sirt1 protein level, and inhibited PERK-eIF2α-ATF4 pathway activation in VSMCs, thus, alleviating VC. The opposite results were obtained in sirt1-knockdown models. Moreover, sirt1 physically interacted with and deacetylated PERK. Mass spectrometry analysis identified lysine K889 as the acetylation site of sirt1, which regulates PERK. Finally, inhibition of sirt1 reduced the effect of terpinen-4-ol on the deacetylation of PERK *in vitro* and *in vivo* and weakened the inhibitory effect of terpinen-4-ol against ER stress-mediated VC.

Conclusions

Terpinen-4-ol inhibits the post-transcriptional modification of PERK at the lysine K889 acetylation site by upregulating sirt1 expression level, thereby ameliorating VC by regulating ER stress. This provides evidence of the molecular mechanism of terpinen-4-ol, which supports its development as a promising therapeutic agent for CKD-VC.

Introduction

Medial vascular calcification (VC) is frequently observed in patients with chronic kidney disease (CKD), and it increases the incidence of cardiovascular events and mortality.[1] VC promotes stiffness of the vascular wall, resulting in increased pulse pressure, left ventricular hypertrophy, and heart failure.[2] Studies have identified the phenotypic switching of vascular smooth muscle cells (VSMCs) as a key event in VC. Osteoblastic differentiation is characterized by the reduction of VSMC markers, such as α-smooth muscle actin (α-SMA) and smooth muscle 22α (SM22α), and the upregulation of the expression of osteogenic markers, such as osteopontin (OPN), runt-related transcription factor 2 (Runx2), and bone morphogenetic protein 2 (BMP2).[3–5] However, the osteogenic/chondral transdifferentiation of VSMCs involves the regulation of multiple complex intracellular signal networks, which is not yet fully understood.

The endoplasmic reticulum (ER), as "the largest factory", is an important organelle in eukaryotic cells, is mainly responsible for lipid biosynthesis, Ca^{2+} homeostasis, and the processing, folding, and secretion of almost all proteins. However, excessive activation of ER stress causes abnormal ER structure and function, thereby promoting the dissociation of the chaperone protein glucose regulatory protein 78 (GRP78) and causing the unfolded protein reaction (UPR) activation.[6, 7] The classic UPR is mainly composed of three pathways: protein kinase RNA-like ER kinase (PERK), inositol-requiring enzyme 1 (IRE1), and activating transcription factor 6 (ATF6).[8, 9] Among them, the PERK-eIF2α-ATF4 signaling is a key signal that induces VC. Phosphorylation of PERK subsequently leads to eukaryotic translation-initiation factor 2α (eIF2α) phosphorylation. Phosphorylated eIF2α can activate downstream activating transcription factor 4 (ATF4) in the nucleus to promote the phenotypic transformation of VSMCs, thereby promoting the development of VC.[10–12] However, the exact molecular mechanism of PERK-eIF2α-ATF4 signaling in CKD-dependent VC is still unclear.

Sirtuin-1 (sirt1) is an NAD^{+}-dependent lysine deacetylase that can deacetylate various proteins and produce nicotinamide as a by-product, which then acts as a negative regulator of sirt1 activities, including regulation of histone and non-histone acetylation in the aging process, apoptosis, and energy metabolism in the anti-stress ability of cells.[13] A recent study showed that sirt1 downregulation promoted calcification of VSMCs under osteogenic conditions[14, 15] and that sirt1-knockdown mice showed accelerated calcification induced by phosphate.[16] Moreover, mechanistically, the downregulation of sirt1 expression promotes the acetylation of the Runx2 promoter region, which increases VSMC calcification.[17] ER stress is an important mechanism in this phenomenon. Increasing evidence shows that sirt1 plays an active role in various ER stress-induced diseases. A study showed that decreased expression of sirt1 can promote the acetylation and phosphorylation of eIF2α, in which sirt1 regulates UPR by regulating eIF2α acetylation on lysine residues K141 and K143 as well as eIF2α phosphorylation on serine Ser51/Ser52. The PERK/eIF2α pathway protects cardiomyocytes from ER stress-induced apoptosis.[18] More recently, Shufang Wu and colleagues[19] showed that sirt1 inhibition promotes both the hyperacetylation and phosphorylation of PERK, and then triggers the PERK-ATF4 signaling of ER stress. However, to date, there are no studies on whether and how sirt1 improves ER stress and inhibits VC at a molecular level by regulating the PERK-eIF2α-ATF4 axis of ER stress.

Terpinen-4-ol, a monomer component, is widely found in most plant essential oils and possesses effective anti-inflammatory, antitumor, and antibacterial effects.[20–24] At present, the protective effect of terpinen-4-ol on VC has not been reported. In this study, we aimed to investigate whether terpinen-4-ol ameliorates VC by regulating the PERK-eIF2α-ATF4 axis of ER stress via sirt1. Our findings would provide a novel mechanism to support the potential of terpinen-4-ol as a promising candidate therapeutic agent for CKD.

Materials And Methods

Relevant materials and reagent information have been described in the supporting materials.

Animal treatment

The animal model was established according to the experimental method of Li et al. and Huang et al.[25, 26] Seven-week-old male C57BL/6J mice were purchased from the Experimental Animal Center of Guizhou Medical University (Guizhou, China). After 1 week of acclimatization period, the mice were divided randomly into four groups and received the following treatment: control group, model group, and two terpinen-4-ol treatment groups. The control group was fed a normal diet, whereas the other groups were fed a high phosphorus diet supplemented with adenine at a dose of 0.2% (w/w). Two terpinen-4-ol treatment groups were administered terpinen-4-ol at a dose of 10 and 20 mg/kg/day respectively. After 6 weeks, all mice were euthanized with an overdose of Pentobarbital sodium (240 mg/kg, IP injection), and the thoracic arteries were collected and stored under specific conditions for further experiments. All animal experiments followed the national guidelines and were approved by the Animal Ethics Committee of the Guizhou Medical University of Technology.

As mentioned earlier, after four weeks of treatment. Grouped as follows: normal saline-treated group (adenine); terpinen-4-ol-treated group (adenine + terpinen-4-ol-H); LV-NC-GFP and saline-treated group (adenine + LV-NC-GFP); LV-NC-GFP and terpinen-4-ol-treated group (adenine + terpinen-4-ol-H + LV-NC-GFP); LV-sirt1 RNAi and saline-treated group (adenine + LV-sirt1 RNAi); and LV-sirt1 RNAi and terpinen-4-ol-treated group (adenine + terpinen-4-ol-H + LV-sirt1 RNAi). A sirt1-knockdown mouse model was established by injecting lentivirus (LV) expressing short hairpin RNA (shRNA) through the tail vein targeting sirt1, which was designed and chemically synthesized by Shanghai GeneChem Co., Ltd. (Shanghai, China). LV carrying negative control gene (LV-NC) expressing green fluorescence protein (NC-GFP) was used as the RNA interference (RNAi) control. The LV-sirt1 RNAi sequence was 5'-GCACCGATCCTCGAACAATTC-3', and the LV-NC sequence was 5'-TTCTCCGAAACGTGTCACGT-3'. LV carrying sirt1 knockdown gene (LV-sirt1 RNAi) or LV-NC was administered at a dose of 5×10^7 via tail vein injection. After the injection of LV-NC or LV-sirt1 RNAi, all mice continued to receive treatment for two weeks and the efficiency of arterial transcription was measured using a fluorescence microscope.

Cell culture and treatment

VSMCs were cultured in a culture medium with DMEM supplemented with 10% FBS, 100 ng/mL FGF cytokine and 1% streptomycin and penicillin at 37 ℃ and 5% CO_2.

VSMCs were inoculated onto a six-well or 60 mm dish and incubated with DMEM + 2% FBS and 10 mmol/L β-GP for 2–14 days to induce VSMC calcification.[27, 28] The culture medium was changed every 2 days. In the drug-treated groups, VSMCs were pre-incubated with terpinen-4-ol at different concentrations for 2 h and then incubated with 10 mmol/L β-GP to induce calcification. In addition, the sirt1 agonist resveratrol, the PERK inhibitor GSK2606414, the ER stress agonist TM, and the ER stress inhibitor 4-PBA were used to study the effect of terpinen-4-ol on β-GP-induced VC. VSMCs were pretreated with resveratrol (50 μmol/L), 4-PBA (5 mmol/L), terpinen-4-ol (20 μmol/L), or GSK2606414 (5 μmol/L) for 2 h, followed by treatment with or without 10 mmol/L β-GP.

Immunohistochemistry

According to standard procedures, artery sections were deparaffinized and rehydrated. Next, the sections were immersed in 0.05 M sodium citrate buffer (pH 8.0) for heat-mediated antigen retrieval and then in 3% hydrogen peroxide for 10 min to remove endogenous peroxidase. After that, the slides were blocked with 10% goat serum at 37 ℃ for 30 min and then incubated with the primary antibody overnight in a humid chamber at 4 ℃. The slides were incubated with an appropriate secondary antibody at 37 ℃ for 30 min and then reacted with 3,3'-diaminobenzidine solution. The tissue sections were observed and then photographed.

Immunofluorescence

VSMCs were seeded in a six-well plate containing coverslips. After treatment, the adherent cells were gently washed with cold PBS three times, fixed with 4% paraformaldehyde for 20 min, and permeabilized with 0.2% Triton-X100 for 15 min. After blocking with goat serum for 40 min, the coverslips were incubated with primary antibodies overnight at 4 ℃. After washing with PBS, the coverslips were incubated with FITC-conjugated secondary antibodies for 1 h at room temperature, followed by incubation with DAPI for 30 min to stain the nucleus. Finally, immunofluorescence images were captured using a Leica DMi8 microscope and the Leica X software (Wetzlar, Germany) at ×200 magnification.

Expression of α-SMA, PERK, and sirt1 in thoracic aortic rings cross sections was determined by immunofluorescent staining. Then, fluorescent images were captured using P250 Pannoramic Scanner (3D Histech, Hungary) and observed by Caseviewer 2.3.

Assessment of ALP activity and calcium content

ALP activity was detected using a specific kit according to the manufacturer's instructions. The results were normalized to the total protein level determined with the BCA protein assay kit to correct the ALP activity in the cells.

Cytosolic Ca^{2+} levels were measured via flow cytometric estimation using Fluo-4 AM.[29, 30] The cells were collected and incubated with 5 μmol/L Fluo-4 AM for 30 minutes at 37℃ in the dark, and then resuspended in 500 μL of phosphate buffered saline (PBS). The fluorescence intensity was recorded at Ex/Em = 488/525 nm using a flow cytometer and analyzed using the NovoExpress software (NovoCyte, ACEA Biosciences, San Diego, CA, USA).

Alizarin red staining

Alizarin Red staining was performed to detect calcium nodules, as described previously.[31, 32] Thoracic aortic rings and VSMCs were fixed with 4% paraformaldehyde for 30 minutes at room temperature. After rinsing with PBS, incubation of 1% alizarin red S (pH 4.2) for 30 min was used to stain followed by rinsing five times with PBS, and then photos were captured with a Leica DMi8 microscope (Wetzlar, Germany).

Sirius Red Staining

The mice thoracic aortic were were fixed with 4% paraformaldehyde and embedded in paraffin. After conventional dewaxing treatment, samples were stained in picro-sirius red solution (0.1% with 1.2% picric acid). Finally, specimens were dehydrated with ethanol. Then, fluorescent images were captured using P250 Pannoramic Scanner (3D Histech, Hungary) and observed by Caseviewer 2.3.

Lentivirus transfection and RNA interference of sirt1

LV overexpressing sirt1 was designed and synthesized by Shanghai Gene Chemistry Co., Ltd. (Shanghai, China). LV expressing GFP was used as a carrier negative control (NC-GFP). According to the manufacturer's instructions, VSMC was transfected with LV-sirt1 or LV-NC. Twenty-four hours after transfection, the medium was removed, and then the cells were incubated in a medium containing β-GP with or without addition of terpinen-4-ol.

Negative control and sirt1 siRNA were designed and synthesized by GenePharma (Shanghai, China). Transfection of siRNA was performed using Lipofectamine 2000 reagent (Invitrogen, Carlsbad, CA, USA) according to the manufacturer’s instructions. The medium was changed after 6 h, and transfected cells were treated as mentioned. The sequences are listed below:sirt1: 5'-UUGUUUCUGGUAAUAAAUCTT-3' (forward);

5'-GAUUUAUUACCAGAAACAATT-3' (reverse). negative control: 5'-UUCUCCGAACGUGUCACGUTT-3' (forward);5'-ACGUGACACGUUCGGAGAATT-3' (reverse).

Quantitative reverse-transcription PCR (qRT-PCR)

Total RNA was extracted from cells, and the expression of related mRNA in VSMCs was determined by quantitative real-time polymerase chain reaction (qRT-PCR) in accordance with the manufacturer's instructions and detected in a CFX96 real-time PCR detection system (Bio-Rad, Hercules, CA, USA). The housekeeping gene GAPDH was used as an endogenous control to normalize the amount of RNA in each

sample. qRT-PCR was performed using primers purchased from Sangon Biotech (Shanghai, China). The primers are listed in Table .

Table Quantitative real-time PCR primers

Gene	Forward primer	Reverse primer
Runx2	TCGGAAAGGGACGAGAG	TTCAAACGCATACCTGCAT
BMP2	AACACAAACAGCGGAAGC	AGCCAGGGGAAAAGGAC
ALP	CCGCAGGATGTGAACTACT	GGTACTGACGGAAGAAGGG
α-SMA	CCGCAAATGCTTCTAAGTC	GCGCTGATCCACAAAAC
GAPDH	GACATGCCGCCTGGAGAAAC	AGCCCAGGATGCCCTTTAGT

Western blotting

After treatment, total extraction of VSMCs or mice thoracic aorta was lysed in lysis buffer containing 99% efficient RIPA tissue/cell fast lysis solution (R0010) and 1% PMSF (R0100) from Solarbio. Protein concentration in the supernatant was detected using a BCA Protein Assay Kit with a microplate spectrophotometer (Thermo Fisher Scientific, Inc.). The total proteins (20–40 μg) were separated by 10% or 12% sodium dodecyl sulfate-polyacrylamide gel electrophoresis (SDS-PAGE) and then transferred to a polyvinylidene fluoride membrane (Cat#T8060; Solarbio). The membranes were blocked with 5% bovine serum albumin for 2 h at room temperature and then incubated with the appropriate primary antibodies overnight at 4 ℃. The membranes were washed with Tris-buffered saline containing Tween 20 and then incubated with secondary antibodies for 2 h at room temperature. The protein blot intensities were quantified using the Image Lab Software (Bio-Rad) and normalized to the housekeeping protein (GAPDH) levels.

Co-immunoprecipitation assay

The total protein was extracted from lysis buffer and incubated with a specific antibody against PERK, sirt1, or acetyl-lysine under frequent mixing overnight at 4 ℃ and added into Protein A/G-agarose beads (Millipore, USA) to generate protein complexes, followed by incubation overnight at 4 ℃ for immunoprecipitation. Immunoprecipitated protein complexes were washed with wash buffer at least six times, boiled in SDS sample buffer for 10 min, and subjected to immunoblotting as described above using an acetyl-lysine antibody (1:200), sirt1 antibody (1:200), or PERK antibody (1:100).

Mass spectrometry analysis

To identify the acetylated sites of PERK, cell lysates were collected and incubated with anti-PERK antibody overnight at 4 ℃ for immunoprecipitation. The immunoprecipitated PERK protein was separated by SDS-PAGE (Figure in the online-only supplemental data). The gel fragments were subjected

to in-gel trypsin digestion, and then extracted with 50% acetonitrile/5% formic acid and 100% acetonitrile. The peptide was dried to completion and resuspended in 2% acetonitrile/0.1% formic acid. The peptide was dissolved in 0.1% formic acid and loaded onto a self-made reverse phase analytical column (length 15 cm, inner diameter 75 μm). The peptides were processed from NSI sources and then tandem mass spectrometry (MS/MS) was performed in Q ExactiveTM Plus (Thermo, USA) connected online to UPLC. Site modifications were performed by PTM Aims (Shanghai, China), as shown in Figure 6e.

Data and statistical analysis

All data are representative of more than three independent experiments, the graph shows the mean + standard deviation. Statistical analysis was performed in GraphPad Prism 7.0 (Inc, La Jolla, CA). multiple sets of data were analyzed through one-way analysis of variance, followed by the Bonferroni *post-hoc* test. Differences between two groups were assessed by Student's *t*-test. *P*-values < 0.05 were considered significantly different ($^{*}P < 0.05$; $^{**}P < 0.01$; $^{***}P < 0.001$).

Results

Terpinen-4-ol improves VC in CKD mice induced by adenine

After 4 weeks of intragastric adenine administration, mice thoracic aorta was calcified, as indicated by increased expression of the VSMC osteogenic phenotype-related markers ALP, BMP2, and Runx2 and decreased expression of the contractile phenotype markers α-SMA; both of these changes were time-dependent (Fig. 1b). Western blotting results showed that the expression of α-SMA in the blood vessels of CKD mice was significantly downregulated, whereas that of BMP2, Runx2, and ALP was upregulated. Nevertheless, terpinen-4-ol upregulated the expression of α-SMA in calcified blood vessels and inhibited the expression of BMP2, Runx2, and ALP (Fig. 1c). These results are consistent with the results of immunofluorescence assay (Fig. 1d). We confirmed that in the thoracic aorta of CKD-VC mice, the expression of Runx2 was upregulated, whereas that of α-SMA was downregulated, and that these effects were reversed by terpinen-4-ol treatment. Alizarin red staining were conducted to evaluate the calcification and of the thoracic aorta of mice in each group. The results showed that the vascular media of CKD mice showed the typical orange-red staining, suggesting calcification of vascular media, this pathological change was reduced in the terpinen-4-ol treatment groups compared with model group. Sirius red staining were conducted to evaluate the expression of collagen fibers in the thoracic aorta of mice. The results showed that compared with the normal group, the accumulation of vascular collagen fibers in the vascular media of CKD mice increased, and the rupture of vascular media elastic fibers, structural disorders, partial irregular arrangement of blood vessels, and loss of normal wavy contractions were observed. After terpinen-4-ol treatment, the vascular collagen content decreases, and the vascular elastic fibers tend to be regular and continuous (Fig. 1e). The above results suggest that terpinen-4-ol reduces vascular calcium salt deposition in CKD mice and inhibits phenotypic switching of VSMC.

Terpinen-4-ol inhibits β-GP-induced phenotypic switching and calcium deposition in VSMCs

It has been shown that 10 mM β-GP enhanced calcium deposition and phenotypic switching in VSMCs.[32] First, we determined changes in the levels of classic osteoblastic differentiation-related markers, and our finding showed significant upregulation of Runx2, ALP, and BMP2 protein levels as well as downregulation of α-SMA protein levels (Fig. 2a) in VSMCs stimulated with β-GP for 3 to 7 days. In addition, after treatment with β-GP, VSMCs showed obvious calcification with many calcified nodules, as revealed by alizarin red S staining (Fig. 2b). Then, we determined the changes in the levels of classic osteoblast differentiation markers (including Runx2, ALP and BMP2) and the VSMC marker α-SMA. Our results showed that terpinen-4-ol enhanced α-SMA expression and reduced Runx2, ALP, and BMP2 expression at both the protein and mRNA levels (Fig. 2c, d). These results showed that co-treatment with terpinen-4-ol reversed the β-GP-induced changes in osteoblastic differentiation-related markers.

The effect of terpinen-4-ol was further confirmed by immunofluorescence analysis. In β-GP-induced VSMCs, the expression and nuclear translocation of Runx2 increased and the expression of α-SMA decreased compared with those in the control; however, these changes were restored by terpinen-4-ol treatment (Fig. 2e). In addition, terpinen-4-ol inhibited the β-GP-induced increase in BMP2 fluorescence intensity (Fig. 2f). VSMCs were stimulated with β-GP and different concentrations of terpinen-4-ol (5 and 20 μM) for 7 days, and the results showed that terpinen-4-ol reduced the calcium deposition of VSMCs (Fig. 2g) and ALP activity (Fig. 2h). However, the increase in intracellular Ca^{2+} content was inhibited by terpinen-4-ol, as confirmed via flow cytometry using the Ca^{2+}-sensitive fluorescence indicator Fluo-4 AM (Fig. 2i). These data suggest that terpinen-4-ol can suppress phenotypic switching and calcium deposition in VSMCs.

Terpinen-4-ol alleviates VC by inhibiting PERK-eIF2α-ATF4 pathway *in vivo* and *in vitro*

Studies have indicated that the CKD environment could induce the activation of the PERK-eIF2α-ATF4 signaling pathway, which leads to ER stress and the development of VC.[33, 34] Taking into account our current findings, we aim to reveal the mechanism of potential endorphins protection. terpinen-4-ol against VC. Therefore, we evaluated the protein expression of the PERK-eIF2α-ATF4 pathway. Western blotting results revealed that the expression of p-PERK, p-eIF2α, and ATF4 increased in CKD mice, but this increase was restored by terpinen-4-ol (Fig. 3a). *In vitro* experiments in VSMC further proved above results(Fig. 3b). The expression of proteins of the PERK-eIF2α-ATF4 pathway was decreased by terpinen-4-ol treatment for 7 days. To examine whether the PERK-eIF2α-ATF4 signaling pathway is related to the effect of terpinen-4-ol on VC, we further used ER stress agonist tunicamycin (TM, 0.1μmol/L) and inhibitor 4-PBA (5 mmol/L) to clarify the effect of terpinen-4-ol on VC.[35, 36] Flow cytometry confirmed that 4-PBA inhibited the β-GP-induced increase in Ca^{2+} in VSMCs (Fig. 3c). The results showed that β-GP and TM activated ER stress, upregulating the expression of osteogenic marker proteins and ER stress-related proteins; however, terpinen-4-ol reversed these effects. Notably, we found that 4-PBA decreased the expression levels of GRP78, p-PERK, p-eIF2α, ATF4, Runx2, ALP, and BMP2, showing no significant difference from those in the group co-treated with terpinen-4-ol and 4-PBA (Fig. 3d, e). Overall, these results indicate that terpinen-4-ol alleviates ER stress *in vivo and in vitro*, which may help improve CKD-VC.

Terpinen-4-ol inhibits VC by upregulating sirt1

It has been reported that the upregulation of sirt1 can improve the VSMC phenotype, whereas the downregulation of sirt1 contributes to CKD-related VC.[37] In the present study, we found that terpinen-4-ol upregulated the expression of sirt1 (Fig. 4a, b). *In vivo* results showed that sirt1 was down-regulated in CKD mouse aortas but was up-regulated in mice treated with terpinen-4-ol (Fig. 4c, d). To determine the regulatory effect of sirt1 on the phenotype transformation of VSMCs, we performed an *in vitro* loss-of-function assay in VSMCs (Fig. 4e). Overexpression of sirt1 was achieved by transfecting VSMCs with a stable LV (Fig. 4g, h). VSMCs transfected with sirt1 siRNA or negative control were cultured with β-GP to induce osteoblast differentiation. The results showed that siRNA-mediated silencing of sirt1 in VSMCs further increased the β-GP-induced increase in calcium salt deposition (Fig. 4f). Silencing of sirt1 further increased the β-GP-induced expression of ALP, BMP2, and Runx2, and further decreased the expression of α-SMA protein. In contrast, LV-mediated sirt1 overexpression decreased the protein levels of osteogenic markers and increased the expression of α-SMA (Fig. 4i). These results indicate that sirt1 plays a negative role in the osteoblast differentiation of VSMCs. We find that no significant changes in the expression of BMP2 and Runx2 were observed after terpinen-4-ol treatment(Fig. 4j). These results once again proved that knockdown sirt1 blocked the effect of terpinen-4-ol on the phenotype transformation of VSMCs.

Terpinen-4-ol alleviates β-GP-induced ER stress in a sirt1-dependent manner

To examine the protective of sirt1 in ER stress-mediated VC, we conducted an experiment using the sirt1 activator resveratrol (50 μmol/L).[38] We noted that terpinen-4-ol and resveratrol reduced the expression of ER stress markers (Fig. 5a). We find that higher expression of p-PERK, p-eIF2α, and ATF4 in the transfected sirt1 siRNA in β-GP-induced VSMCs. It is worth noting that in VSMCs with silenced sirt1, no significant changes were observed after terpinen-4-ol treatment(Fig. 5b). In contrast, sirt1 overexpression further decreased the protein levels of ER stress markers in VSMCs (Fig. 5c).These results indicate that terpinen-4-ol could regulate PERK-eIF2α-ATF4 pathway to inhibit VC by upregulating the expression of sirt1.

We further examined the effects of sirt1 gene silencing on VC in adenine-induced CKD mice. Knockdown of the sirt1 gene *in vivo* was confirmed by both fluorescence microscopy and western blotting (Fig. 4d). After 6 weeks of adenine administration, western blotting results showed no change in the expression of ER stress and osteogenic differentiation marker proteins following NC-GFP injection compared with that in the normal group. Compared with NC-GFP, LV-sirt1 RNAi decreased the expression of α-SMA and increased the expression of BMP2, Runx2, p-PERK, p-eIF2α, and ATF4, suggesting that sirt1 knockdown promoted ER stress and VC, consistent with the *in vitro* results. Moreover, LV-sirt1 RNAi injection significantly reduced the expression of sirt1 and the terpinen-4-ol-induced decrease in the expression of ER stress and VC-related markers in the aorta of adenine-fed mice, once again proving that sirt1 is a key signal involved in ER stress and may be an important molecular target of terpinen-4-ol in inhibiting VC. We also found, through immunofluorescence staining, that PERK and sirt1 were co-localized in the thoracic aorta of CKD-VC mice (Fig. 5f). These results suggest that terpinen-4-ol can improve β-GP-

induced ER stress by downregulating the expression of sirt1 and that sirt1 knockdown diminishes the ameliorative effect of terpinen-4-ol on ER stress.

Terpinen-4-ol improves ER stress-induced VC through sirt1-mediated PERK deacetylation

To confirm the role of PERK in ER stress-induced VC, we performed an experiment with terpinen-4-ol and the PERK inhibitor GSK2606414 (5 μmol/L).[39] The results showed that GSK2606414 suppressed the expression of ER stress markers and VC-related proteins.. In order to study the mechanism of sirt1 attenuating PERK signal pathway, the acetylated protein on the lysine residues were removed from the VSMC lysate. PERK is present in the anti-acetyl-lysine immunoprecipitate. Mutual immunoprecipitation further confirmed the acetylation of PERK (Fig. 6b). Moreover, knockdown of sirt1 greatly increased the acetylation of PERK (Fig. 6c). We also confirmed that sirt1 and PERK existed in a protein binding mode (Fig. 6d). The immunoprecipitation results showed that β-GP treatment promoted PERK acetylation, and terpinen-4-ol can reverse this effect by inhibiting the acetylation modification of PERK (Fig. 6e). Consistent with the *in vitro* findings, terpinen-4-ol inhibited PERK acetylation in CKD mice (Fig. 6f). In VSMCs transfected with an empty vector, β-GP exposure increased PERK acetylation, which was significantly reversed by terpinen-4-ol treatment. In sirt1 siRNA-transfected VSMCs treated with or without terpinen-4-ol, PERK acetylation was increased (Fig. 6g). The *in vitro* results also showed that the inhibitory effect of terpinen-4-ol on PERK acetylation was significantly blocked by LV-sirt1 RNAi injection (Fig. 6h). To identify the sites of PERK acetylation, PERK was subjected to immunoprecipitation, followed by proteolytic digestion and nano-LC-MS/MS analysis (Fig. 6i). The analysis revealed different trypsin-cleaved peptides near K889 (peptides ENLKDWMNR). In addition, an increase of 42 011 Da was observed in the mass of lysine K889, which is equivalent to an increase of an acetyl group. These results revealed not only that the PERK protein was acetylated but also that its prominent acetylation site was lysine K889. The PERK protein sequence is highly conserved among species(e.g. R. norvegicus, H. sapiens, D. Rerio and X. Tropicalis et.al) (Fig. 6j). The structure of PERK was predicted using I-TASSER, and the pymol algorithm was constructed for visualization. The crystal structure of PERK showed that K889 (red) was located in the protein kinase-like domain (yellow) (Fig. 6k). The above results suggest that terpinen-4-ol improves ER-induced CKD-VC by mediating PERK deacetylation through sirt1.

Discussion

CKD-VC threatens human health owing to its high morbidity and mortality, and this disease is difficult to treat. Mechanistically, the osteogenic phenotype transformation of VSMCs promotes the development of VC.[40–42] Therefore, preventing the phenotype switching of VSMCs may be a new therapeutic option for CKD-VC. Terpinen-4-ol, a monoterpene from aromatic plants, has previously been investigated for therapeutic potentials against VC by biological approaches. Our previous research showed that terpinen-4-ol inhibits oxidative stress damage in VSMCs induced by high glucose.[43] Thus, we purposed to elucidate the effect of terpinen-4-ol on CKD-VC. Disturbance of mineral homeostasis and abnormal deposition of calcium and phosphorus in blood vessel walls are core processes of VC.[44–46] Our present results showed that terpinen-4-ol reduced calcium deposition and ALP activity in CKD mouse

arteries. Furthermore, our results confirmed that terpinen-4-ol inhibits the β-GP-induced increases in calcium deposition, calcium concentration, and ALP activity in rat VSMCs. However, evidence has shown that VC is not simply caused by calcium salt deposition and that phenotype switching of VSMCs. We showed that terpinen-4-ol inhibited the phenotype switching of VSMCs.

Accumulating evidence has indicated that ER stress contributes to the progression of CKD through increased VSMC differentiation.[47] It is well established that the PERK-eIF2a-ATF4-CHOP pathway is upregulated in animal models of VC.[11, 48] *In vitro* models suggest that ER stress also increases the expression of ATF4, which binds to the Runx2 promoter, affecting VSMCs calcification.[49–51] In order to clarify the relationship between ER stress and VC, we used 4-PBA, a classic ER stress inhibitor. 4-PBA significantly alleviated VC-related protein levels. This indicates that ER stress participates in the development of VC. Moreover, our results also indicated that terpinen-4-ol decreased the levels of ER stress markers and VC-related marker proteins, which were increased by the ER stress inducer TM. Taken together, this study showed for the first time that the protective effects of terpinen-4-ol was related to the inhibition of the PERK signal pathway. However, it is not clear whether IRE1 and ATF6 signaling pathways of ER stress are related to the effects of terpinen-4-ol on VC, thus further research is needed.

Numerous studies have shown that sirt1 could attenuate VC by reversing the osteoblastic differentiation of VSMCs.[52] More importantly, the downregulation of sirt1 contributes to CKD-associated VC.[15, 53] In addition, sirt1 activators, such as resveratrol, [54–56] have been proposed as therapeutic strategies for treating and preventing VC, as they can alleviate the calcification of VSMCs by increasing the expression of the calcification inhibitors such as OPG and OPN. More importantly, sirt1 directly regulates VC through the deacetylation of the Runx2 promoter.[14] Consequently, sirt1 possesses anti-calcification activity. Consistent with these findings, our study confirmed that sirt1 expression was significantly lower in β-GP-induced VSMCs and in the thoracic aorta of CKD mice, but sirt1 expression was upregulated by terpinen-4-ol treatment. Moreover, we used LV-sirt1 to induce sirt1 overexpression, and our results indicated that sirt1 inhibits the osteoblast differentiation of VSMCs, as evidenced by the reduced expression of osteoblast differentiation markers. In contrast, siRNA-mediated silencing of sirt1 promoted osteoblast differentiation of VSMCs. Altogether, these data suggest that sirt1 functions as a negative regulator of osteoblast differentiation in CKD-VC. Upregulation of sirt1 leads to inhibition of IRE1α, PERK, and ATF6 signaling pathways that activate ER stress.[57–60] We observed that pre-incubation of VSMCs with terpinen-4-ol or the sirt1 agonist resveratrol and transfection of VSMCs with LV overexpressing sirt1 (LV-sirt1) decreased β-GP-induced calcium salt deposition, inhibited ER stress, and improved the phenotypic transformation of VSMCs. These findings following *in vitro* silencing of sirt1 and *in vivo* injection of LV-sirt1 RNAi are contrary to overexpressing sirt1 results. Therefore, our results provide that terpinen-4-ol alleviates β-GP-induced ER stress and osteoblast phenotypic switching of VSMCs in a sirt1-dependent manner

The ability of cells to respond to ER stress is essential for cell survival, but the unrecoverable level of ER stress could lead to VC.[61, 62] The knockdown of the PERK-eIF2α-ATF4-CHOP pathway blocks osteoblastic differentiation in VSMCs. PERK siRNA reduced the protein levels of PERK and its

downstream target, p-eIF2α, which notably diminished calcification and ALP activity.[34, 49] We found that the PERK inhibitor GSK2606414 suppressed ER stress and reversed the phenotypic switching of VSMCs. PERK is a strong positive regulator of ER stress and VC. Acetylation and deacetylation of proteins modulates a wide variety of cellular biological processes, such as cell proliferation, gene transcription, apoptosis, and protein stability.[63–66] Acetylation modification of proteins is closely related to numerous diseases, including cancer and cardiovascular disease. Immunoprecipitation experiments revealed that PERK protein acetylation was high in the thoracic aorta and calcified VSMCs of CKD mice. This difference in expression suggests that acetylated PERK may play a role in VC. Terpinen-4-ol treatment reduced the PERK acetylation. Thus, our results showed that sirt1 specifically interacts with PERK, reducing PERK acetylation. sirt1 is a deacetylase, and a recent study showed that sirt1 deacetylates PERK in chondrocyte hypertrophy.[19] Injection of LV-sirt1 RNAi in vivo and sirt1 siRNA silencing in vitro promoted PERK hyperacetylation and then triggered the PERK-ATF4-ATF4 axis of ER stress. We performed mass spectrometry analysis to corroborate this finding and to map the acetylation sites, and our results showed acetylation of PERK at lysine K889 in rat VSMCs. As the K889 site of PERK is highly conserved in many mammals, our results also suggest that PERK acetylation at the K889 site may regulate VC caused by ER stress. Interestingly, we found that terpinen-4-ol reduced the deacetylation of PERK to alleviate ER stress and osteoblast phenotypic switching of VSMCs in a sirt1-dependent manner.

Limitations

The present study has several limitations. We used LV to knockdown sirt1 in CKD mouse aortas. Although the results of fluorescence microscopy and western blotting assay proved that sirt1 was effectively knocked-down in the mouse thoracic aorta, there are currently many studies using LV overexpression or interference of genes in the thoracic aorta, but it is better than when experiments were conducted on sirt1-/- knockout mice. In addition, we proved that sirt1 can regulate the acetylation/deacetylation of PERK, and PERK is acetylated at position K889; therefore, the function of acetylated PERK protein needs to be further clarified by a point mutation in the next step.

Conclusion

In summary, our study showed that terpinen-4-ol can inhibit the ER-mediated phenotypic transformation of VSMCs by regulating PERK acetylation modification by sirt1. As shown in Fig. 7, this indicates that sirt1 is essential for terpinen-4-ol alleviated VC, which provides a novel mechanism supporting terpinen-4-ol or activation of sirt1 signaling as a promising clinical therapeutic agent or strategy, respectively, for the treatment of CKD-VC.

Abbreviations

ALP: alkaline phosphatase; BMP2: bone morphogenetic protein 2; VSMC: vascular smooth muscle cell; Runx2: runt-related transcription factor 2; α-SMA: α-smooth muscle actin; SM22α: smooth muscle 22α;

OPN: osteopontin; CKD: chronic kidney disease; VC: vascular calcification; ER: endoplasmic reticulum; GRP78: glucose regulatory protein 78; PERK: protein kinase RNA-like endoplasmic reticulum kinase; UPR: unfolded protein reaction; IRE1: inositol-requiring enzyme 1; ATF6: activating transcription factor 6; eIF2α: eukaryotic translation-initiation factor 2α; β-GP: β-glycerophosphate; ATF4: activating transcription factor 4; sirt1: sirtuin-1; TM: tunicamycin; 4-PBA: 4-phenylbutyric acid.

Declarations

Acknowledgements

Not applicable.

Author contributions

Y-YZ and L H designed and performed experiments, analyzed data, and wrote the manuscript. M-XT and M H performed part of the experiments and analyzed data. Y C and D P provided general support and manuscript preparation. J-QP corrected grammatical and typing errors and revised the final manuscript. X-CS designed the experiment and revised the manuscript. All authors read and approved the final manuscript.

Sources of Funding

This work was supported by the National Natural Science Foundation of China (grant numbers 81560811, 82060775, 81760725, U1812403-4-4), the Guizhou Provincial Natural Science Foundation (No. [2020]1Z069), the Fund of High Level Innovation Talents [grant number 2015-4029], the base of international scientific and technological cooperation of Guizhou Province [No. (2017)5802], the Guizhou Provincial Key Technology R&D Program [grant no. (2020)4Y093], the Guizhou Province Graduate Research Fund [Qianjiaohe Support YJSCXJH (2019)074], the Guizhou Province College Student Innovation and Entrepreneurship Training Program [grant no. (2020)S202010660029].

Availability of data and materials

The datasets used and analyzed during the current study are available from the corresponding author on reasonable request.

Ethics approval and consent to participate

All animal experiments followed the national guidelines and were approved by the Animal Ethics Committee of the Guizhou Medical University of Technology (NO. Qian 2000166).

Consent for publication

All authors gave consent for publication.

Competing interests

The authors declare that they have no competing interests.

Authors' information

[1] The State Key Laboratory of Functions and Applications of Medicinal Plants，Guizhou Medical University, University Town, Guian New District, Guizhou, China. [2] Department of Clinical Pharmacy, School of Pharmaceutical Sciences, Guizhou Medical University, University Town, Guian New District, Guizhou, China. [3] Department of Pharmacology of Materia Medica (the High Educational Key Laboratory of Guizhou Province for Natural Medicinal Pharmacology and Druggability,the High Efficacy Application of Natural Medicinal Resources Engineering Center of Guizhou Province), Guizhou Medical University, University Town, Guian New District, Guizhou, China. [4] The Key Laboratory of Optimal Utilization of Natural Medicine Resources, School of Pharmaceutical Sciences, Guizhou Medical University, University Town, Guian New District, Guizhou, China.

References

1. Shanahan CM CM, Kapustin A, Journal club. Arterial calcification in chronic kidney disease: key roles for calcium and phosphate. Kidney Int. 2011; 80:1250-1.
2. Alani H, Tamimi A, Tamimi N. Cardiovascular co-morbidity in chronic kidney disease: Current knowledge and future research needs. World J Nephrol. 2014; 3:156-68.
3. Patel JJ, Bourne LE, Davies BK, Arnett TR, MacRae VE, Wheeler-Jones CP, et al. Differing calcification processes in cultured vascular smooth muscle cells and osteoblasts. Exp Cell Res. 2019; 380:100-13.
4. Zhu Y, Ma WQ, Han XQ, Wang Y, Wang X, Liu NF. Advanced glycation end products accelerate calcification in VSMCs through HIF-1α/PDK4 activation and suppress glucose metabolism. Sci Rep. 2018; 8:13730.
5. Sun Y, Byon CH, Yuan K, Chen J, Mao X, Heath JM, et al. Smooth muscle cell-specific runx2 deficiency inhibits vascular calcification. Circ Res. 2012; 111:543-52.
6. Chen MT, Huang RL, Ou LJ, Chen YN, Men L, Chang X, et al. Pollen Typhae Total Flavone Inhibits Endoplasmic Reticulum Stress-Induced Apoptosis in Human Aortic-Vascular Smooth Muscle Cells through Down-Regulating PERK-eIF2α-ATF4-CHOP Pathway. Chin J Integr Med. 2019; 25:604-12.
7. Park K, Lee SE, Shin KO, Uchida Y. Insights into the role of endoplasmic reticulum stress in skin function and associated diseases. Febs j. 2019; 286:413-25.
8. Ghosh R, Colon-Negron K, Papa FR. Endoplasmic reticulum stress, degeneration of pancreatic islet β-cells, and therapeutic modulation of the unfolded protein response in diabetes. Mol Metab. 2019; 27:S60-8.
9. Sankrityayan H, Oza MJ, Kulkarni YA, Mulay SR, Gaikwad AB. ER stress response mediates diabetic microvascular complications. Drug Discov Today 2019; 24:2247-57.

10. Duan X, Zhou Y, Teng X, Tang C, Qi Y. Endoplasmic reticulum stress-mediated apoptosis is activated in vascular calcification. Biochem Biophys Res Commun. 2009; 387:694-9.
11. Masuda M, Miyazaki-Anzai S, Levi M, Ting TC, Miyazaki M. PERK-eIF2α-ATF4-CHOP signaling contributes to TNFα-induced vascular calcification. J Am Heart Assoc. 2013; 2:e000238.
12. Moore PC, Qi JY, Thamsen M, Ghosh R, Peng J, Gliedt MJ, et al. Parallel Signaling through IRE1α and PERK Regulates Pancreatic Neuroendocrine Tumor Growth and Survival. Cancer Res. 2019; 79:6190-203.
13. Lu CL, Liao MT, Hou YC, Fang YW, Zheng CM, Liu WC, et al. Sirtuin-1 and Its Relevance in Vascular Calcification. Int J Mol Sci. 2020; 21.
14. Bartoli-Leonard F, Wilkinson FL, Schiro A, Inglott FS, Alexander MY, Weston R. Suppression of SIRT1 in Diabetic Conditions Induces Osteogenic Differentiation of Human Vascular Smooth Muscle Cells via RUNX2 Signalling. Sci Rep. 2019; 9:878.
15. Takemura A, Iijima K, Ota H, Son BK, Ito Y, Ogawa S, et al. Sirtuin 1 retards hyperphosphatemia-induced calcification of vascular smooth muscle cells. Arterioscler Thromb Vasc Biol. 2011; 31:2054-62.
16. Akiyoshi T, Ota H, Iijima K, Son BK, Kahyo T, Setou M, et al. A novel organ culture model of aorta for vascular calcification. Atherosclerosis. 2016; 244:51-8.
17. Yu L, Li S, Tang X, Li Z, Zhang J, Xue X, et al. Diallyl trisulfide ameliorates myocardial ischemia-reperfusion injury by reducing oxidative stress and endoplasmic reticulum stress-mediated apoptosis in type 1 diabetic rats: role of SIRT1 activation. Apoptosis. 2017; 22:942-54.
18. Prola A, Pires Da Silva J, Guilbert A, Lecru L, Piquereau J, Ribeiro M, et al: SIRT1 protects the heart from ER stress-induced cell death through eIF2α deacetylation. Cell Death Differ. 2017; 24:343-56.
19. Kang X, Yang W, Wang R, Xie T, Li H, Feng D, et al. Sirtuin-1 (SIRT1) stimulates growth-plate chondrogenesis by attenuating the PERK-eIF-2α-CHOP pathway in the unfolded protein response. J Biol Chem. 2018, 293:8614-25.
20. Nakayama K, Murata S, Ito H, Iwasaki K, Villareal MO, Zheng YW, et al. Terpinen-4-ol inhibits colorectal cancer growth via reactive oxygen species. Oncol Lett. 2017; 14:2015-24.
21. Banjerdpongchai R, Khaw-On P. Terpinen-4-ol induces autophagic and apoptotic cell death in human leukemic HL-60 cells. Asian Pac J Cancer Prev. 2013; 14:7537-42.
22. Ning J, Xu L, Zhao Q, Zhang YY, Shen CQ. The Protective Effects of Terpinen-4-ol on LPS-Induced Acute Lung Injury via Activating PPAR-γ. Inflammation. 2018; 41:2012-7.
23. Santos-Nascimento TD, Veras KM, Moreira-Júnior L, Coelho-de-Souza AN, Pereira-Gonçalves Á, Silva-Dos-Santos NM, et al. Monoterpenoid terpinen-4-ol inhibits voltage-dependent Na(+) channels of small dorsal root ganglia rat neurons. Chem Biol Interact. 2020; 315:108890.
24. Chen D, Wang J, Sullivan DA, Kam WR, Liu Y. Effects of Terpinen-4-ol on Meibomian Gland Epithelial Cells In Vitro. Cornea. 2020; 39:1541-6.

25. Li XY, Li QM, Fang Q, Zha XQ, Pan LH, Luo JP. Laminaria japonica Polysaccharide Inhibits Vascular Calcification via Preventing Osteoblastic Differentiation of Vascular Smooth Muscle Cells. J Agric Food Chem. 2018; 66:1821-7.
26. Huang LH, Liu H, Chen JY, Sun XY, Yao ZH, Han J, et al. Seaweed Porphyra yezoensis polysaccharides with different molecular weights inhibit hydroxyapatite damage and osteoblast differentiation of A7R5 cells. Food Funct. 2020; 11:3393-409.
27. Wang S, Hu S, Wang J, Liu Y, Zhao R, Tong M, et al. Conditioned medium from bone marrow-derived mesenchymal stem cells inhibits vascular calcification through blockade of the BMP2-Smad1/5/8 signaling pathway. Stem Cell Res Ther. 2018;:160.
28. Liu Y, Lin F, Fu Y, Chen W, Liu W, Chi J, et al. Cortistatin inhibits arterial calcification in rats via GSK3β/β-catenin and protein kinase C signalling but not c-Jun N-terminal kinase signalling. Acta Physiol (Oxf). 2018; 223:e13055.
29. Bai YL, Xu JS, Tian T, Zhang JX, Cui LW, Zhang HR, et al. Effect and mechanism of intermittent alkaline stimulation on high phosphorus induced calcification in vascular smooth muscle cells of rats. Zhonghua Xin Xue Guan Bing Za Zhi. 2017; 45:519-25.
30. Zhang CY, Sun XY, Ouyang JM, Gui BS. Diethyl citrate and sodium citrate reduce the cytotoxic effects of nanosized hydroxyapatite crystals on mouse vascular smooth muscle cells. Int J Nanomedicine. 2017; 12:8511-25.
31. Zhou P, Zhang X, Guo M, Guo R, Wang L, Zhang Z, et al. Ginsenoside Rb1 ameliorates CKD-associated vascular calcification by inhibiting the Wnt/β-catenin pathway. J Cell Mol Med. 2019; 23:7088-98.
32. Mahmoud AM, Jones AM, Sidgwick GP, Arafat AM, Alexander YM, Wilkinson FL. Small Molecule Glycomimetics Inhibit Vascular Calcification via c-Met/Notch3/HES1 Signalling. Cell Physiol Biochem. 2019; 53:323-36.
33. Chang JR, Sun N, Liu Y, Wei M, Zhao Y, Gan L, et al. Erythropoietin attenuates vascular calcification by inhibiting endoplasmic reticulum stress in rats with chronic kidney disease. Peptides. 2020; 123:170181.
34. Zhang R, Jiang M, Zhang J, Qiu Y, Li D, Li S, et al. Regulation of the cerebrovascular smooth muscle cell phenotype by mitochondrial oxidative injury and endoplasmic reticulum stress in simulated microgravity rats via the PERK-eIF2α-ATF4-CHOP pathway. Biochim Biophys Acta Mol Basis Dis. 2020; 1866:165799.
35. Kwon MY, Hwang N, Lee SJ, Chung SW. Nucleotide-binding oligomerization domain protein 2 attenuates ER stress-induced cell death in vascular smooth muscle cells. BMB Rep. 2019; 52:665-70.
36. Lin H, Ni T, Zhang J, Meng L, Gao F, Pan S, et al. Knockdown of Herp alleviates hyperhomocysteinemia mediated atherosclerosis through the inhibition of vascular smooth muscle cell phenotype switching. Int J Cardiol. 2018; 269:242-9.
37. Chen Y, Zhang LS, Ren JL, Zhang YR, Wu N, Jia MZ, et al. Intermedin(1-53) attenuates aging-associated vascular calcification in rats by upregulating sirtuin 1. Aging (Albany NY). 2020; 12:5651-

74.

38. Almajdoob S, Hossain E, Anand-Srivastava MB. Resveratrol attenuates hyperproliferation of vascular smooth muscle cells from spontaneously hypertensive rats: Role of ROS and ROS-mediated cell signaling. Vascul Pharmacol. 2018; 101:48-56.
39. Guo J, Ren R, Sun K, Yao X, Lin J, Wang G, et al. PERK controls bone homeostasis through the regulation of osteoclast differentiation and function. Cell Death Dis. 2020; 11:847.
40. Alesutan I, Voelkl J, Feger M, Kratschmar DV, Castor T, Mia S, et al. Involvement Of Vascular Aldosterone Synthase In Phosphate-Induced Osteogenic Transformation Of Vascular Smooth Muscle Cells. Sci Rep. 2017; 7:2059.
41. Voelkl J, Lang F, Eckardt KU, Amann K, Kuro OM, Pasch A, et al. Signaling pathways involved in vascular smooth muscle cell calcification during hyperphosphatemia. Cell Mol Life Sci. 2019; 76:2077-91.
42. Cozzolino M, Ciceri P, Galassi A, Mangano M, Carugo S, Capelli I, et al. The Key Role of Phosphate on Vascular Calcification. Toxins (Basel). 2019; 11.
43. Wu CS, Chen YJ, Chen JJ, Shieh JJ, Huang CH, Lin PS, et al. Terpinen-4-ol Induces Apoptosis in Human Nonsmall Cell Lung Cancer In Vitro and In Vivo. Evid Based Complement Alternat Med. 2012; 2012:818261.
44. Stabley JN, Towler DA. Arterial Calcification in Diabetes Mellitus: Preclinical Models and Translational Implications. Arterioscler Thromb Vasc Biol 2017, 37(2):205-17.
45. Gomez D, Owens GK. Smooth muscle cell phenotypic switching in atherosclerosis. Cardiovasc Res. 2012; 95:156-64.
46. Huang M, Zheng L, Xu H, Tang D, Lin L, Zhang J, et al. Oxidative stress contributes to vascular calcification in patients with chronic kidney disease. J Mol Cell Cardiol. 2020; 138:256-68.
47. Panda DK, Bai X, Sabbagh Y, Zhang Y, Zaun HC, Karellis A, et al. Defective interplay between mTORC1 activity and endoplasmic reticulum stress-unfolded protein response in uremic vascular calcification. Am J Physiol Renal Physiol. 2018; 314:F1046-61.
48. Miyazaki-Anzai S, Masuda M, Demos-Davies KM, Keenan AL, Saunders SJ, Masuda R, et al. Endoplasmic reticulum stress effector CCAAT/enhancer-binding protein homologous protein (CHOP) regulates chronic kidney disease-induced vascular calcification. J Am Heart Assoc. 2014; 3:e000949.
49. Masuda M, Ting TC, Levi M, Saunders SJ, Miyazaki-Anzai S, Miyazaki M. Activating transcription factor 4 regulates stearate-induced vascular calcification. J Lipid Res. 2012; 53:1543-52.
50. Zhang K, Wang M, Li Y, Li C, Tang S, Qu X, et al. The PERK-EIF2α-ATF4 signaling branch regulates osteoblast differentiation and proliferation by PTH. Am J Physiol Endocrinol Metab. 2019; 316(4):e590-604.
51. Liberman M, Johnson RC, Handy DE, Loscalzo J, Leopold JA. Bone morphogenetic protein-2 activates NADPH oxidase to increase endoplasmic reticulum stress and human coronary artery smooth muscle cell calcification. Biochem Biophys Res Commun. 2011; 413:436-41.

52. Wan W, Ding Y, Xie Z, Li Q, Yan F, Budbazar E, et al. PDGFR-β modulates vascular smooth muscle cell phenotype via IRF-9/SIRT-1/NF-κB pathway in subarachnoid hemorrhage rats. J Cereb Blood Flow Metab. 2019; 39:1369-80.
53. Bartoli-Leonard F, Wilkinson FL, Schiro A, Inglott FS, Alexander MY, Weston R. Loss of SIRT1 in diabetes accelerates DNA damage induced vascular calcification. Cardiovasc Res. 2020.
54. Wallerath T, Deckert G, Ternes T, Anderson H, Li H, Witte K, et al. Resveratrol, a polyphenolic phytoalexin present in red wine, enhances expression and activity of endothelial nitric oxide synthase. Circulation. 2002; 106:1652-8.
55. Zhang C, Feng Y, Qu S, Wei X, Zhu H, Luo Q, et al. Resveratrol attenuates doxorubicin-induced cardiomyocyte apoptosis in mice through SIRT1-mediated deacetylation of p53. Cardiovasc Res. 2011; 90:538-45.
56. Milne JC, Lambert PD, Schenk S, Carney DP, Smith JJ, Gagne DJ, et al. Small molecule activators of SIRT1 as therapeutics for the treatment of type 2 diabetes. Nature. 2007; 450:712-6.
57. Pires Da Silva J, Monceaux K, Guilbert A, Gressette M, Piquereau J, Novotova M, et al. SIRT1 Protects the Heart from ER Stress-Induced Injury by Promoting eEF2K/eEF2-Dependent Autophagy. Cells. 2020; 9.
58. Feng K, Ge Y, Chen Z, Li X, Liu Z, Li X, et al. Curcumin Inhibits the PERK-eIF2α-CHOP Pathway through Promoting SIRT1 Expression in Oxidative Stress-induced Rat Chondrocytes and Ameliorates Osteoarthritis Progression in a Rat Model. Oxid Med Cell Longev. 2019; 2019:8574386.
59. Lee J, Hong SW, Kwon H, Park SE, Rhee EJ, Park CY, et al. Resveratrol, an activator of SIRT1, improves ER stress by increasing clusterin expression in HepG2 cells. Cell Stress Chaperones. 2019, 24:825-33.
60. Feng K, Chen Z, Pengcheng L, Zhang S, Wang X. Quercetin attenuates oxidative stress-induced apoptosis via SIRT1/AMPK-mediated inhibition of ER stress in rat chondrocytes and prevents the progression of osteoarthritis in a rat model. J Cell Physiol. 2019; 234:18192-205.
61. Lee SJ, Lee IK, Jeon JH. Vascular Calcification-New Insights Into Its Mechanism. Int J Mol Sci. 2020; 21.
62. Zhu Q, Guo R, Liu C, Fu D, Liu F, Hu J, et al. Endoplasmic Reticulum Stress-Mediated Apoptosis Contributing to High Glucose-Induced Vascular Smooth Muscle Cell Calcification. J Vasc Res. 2015; 52:291-8.
63. Narita T, Weinert BT, Choudhary C: Functions and mechanisms of non-histone protein acetylation. Nat Rev Mol Cell Biol. 2019; 20:156-74.
64. Pons D, de Vries FR, van den Elsen PJ, Heijmans BT, Quax PH, Jukema JW. Epigenetic histone acetylation modifiers in vascular remodelling: new targets for therapy in cardiovascular disease. Eur Heart J. 2009; 30:266-77.
65. Singh BN, Zhang G, Hwa YL, Li J, Dowdy SC, Jiang SW. Nonhistone protein acetylation as cancer therapy targets. Expert Rev Anticancer Ther. 2010; 10:935-54.

66. Hyndman KA. Histone Deacetylases in Kidney Physiology and Acute Kidney Injury. Semin Nephrol. 2020; 40:138-47.

Figures

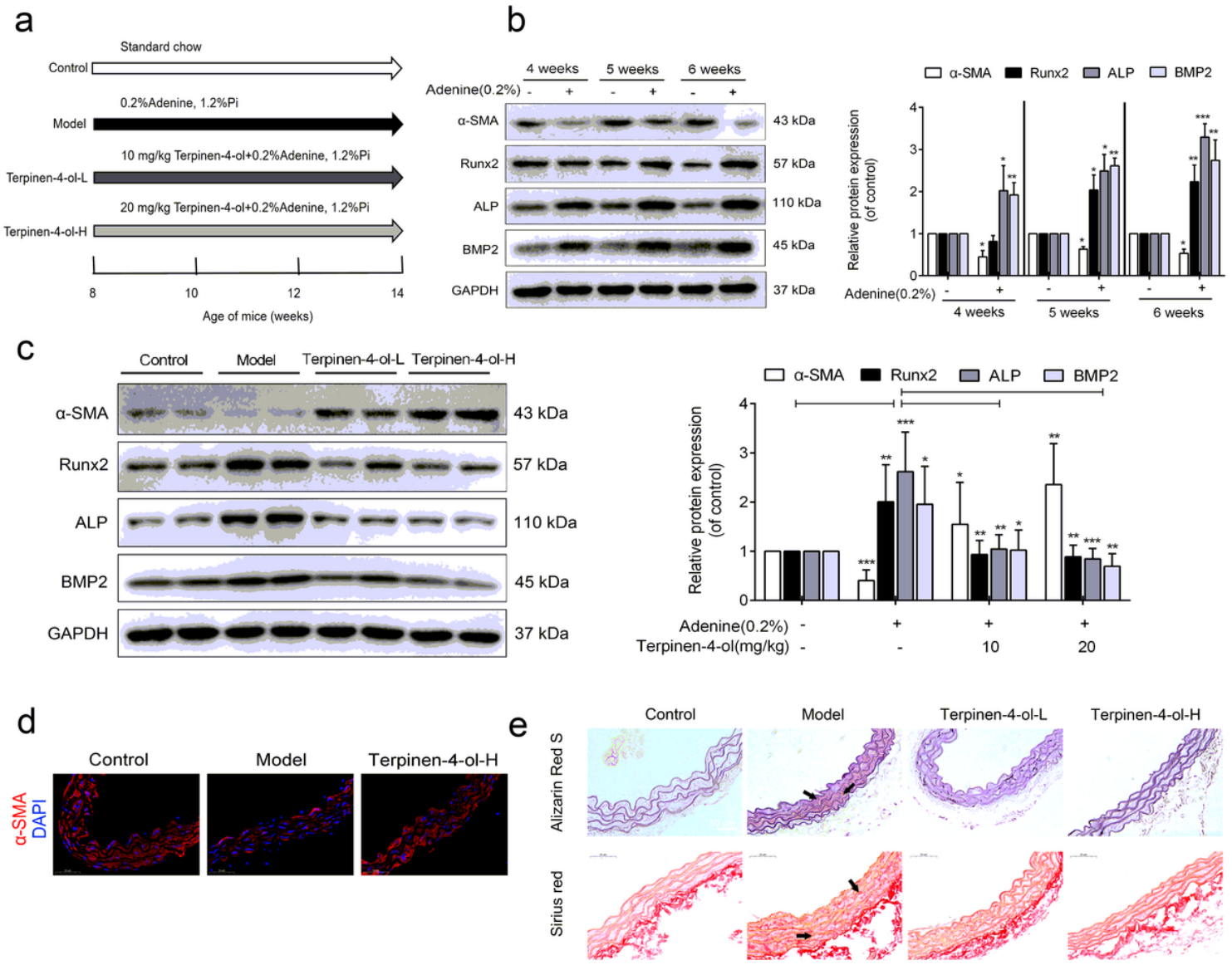

Figure 1

Terpinen-4-ol improves VC in CKD mice induced with adenine. (a) C57BL/6J mice in four groups (n=10/group) were subjected to the indicated treatment for 6 weeks. Control: standard chow; Model: Adenine (0.2%, 0.1 mL/10 g/day, intragastric) + high-phosphorus feed (1.2%); Terpinen-4-ol-L: terpinen-4-ol treatment (10 mg/kg/day) by gavage for 6 weeks; Terpinen-4-ol-H: terpinen-4-ol treatment (20 mg/kg/day) by gavage for 6 weeks. (b) Western blotting results showed the levels of α-SMA, Runx2, ALP, and BMP2 in mouse aortas treated with or without adenine for 4-6 weeks. (c) Western blotting analysis of α-SMA, Runx2, ALP, and BMP2 in mouse aorta tissues; GAPDH was used as a loading control. (d)

Expression of α-SMA in mouse aortas was determined by immunofluorescent staining of aortic root cross-sections (scale bar: 50 μm). (e) Alizarin red staining and sirius red staining of mouse aortas (scale bar: 50 μm). All data represent the mean ± SEM of more than three experiments. *P < 0.05, **P < 0.01, ***P < 0.001.

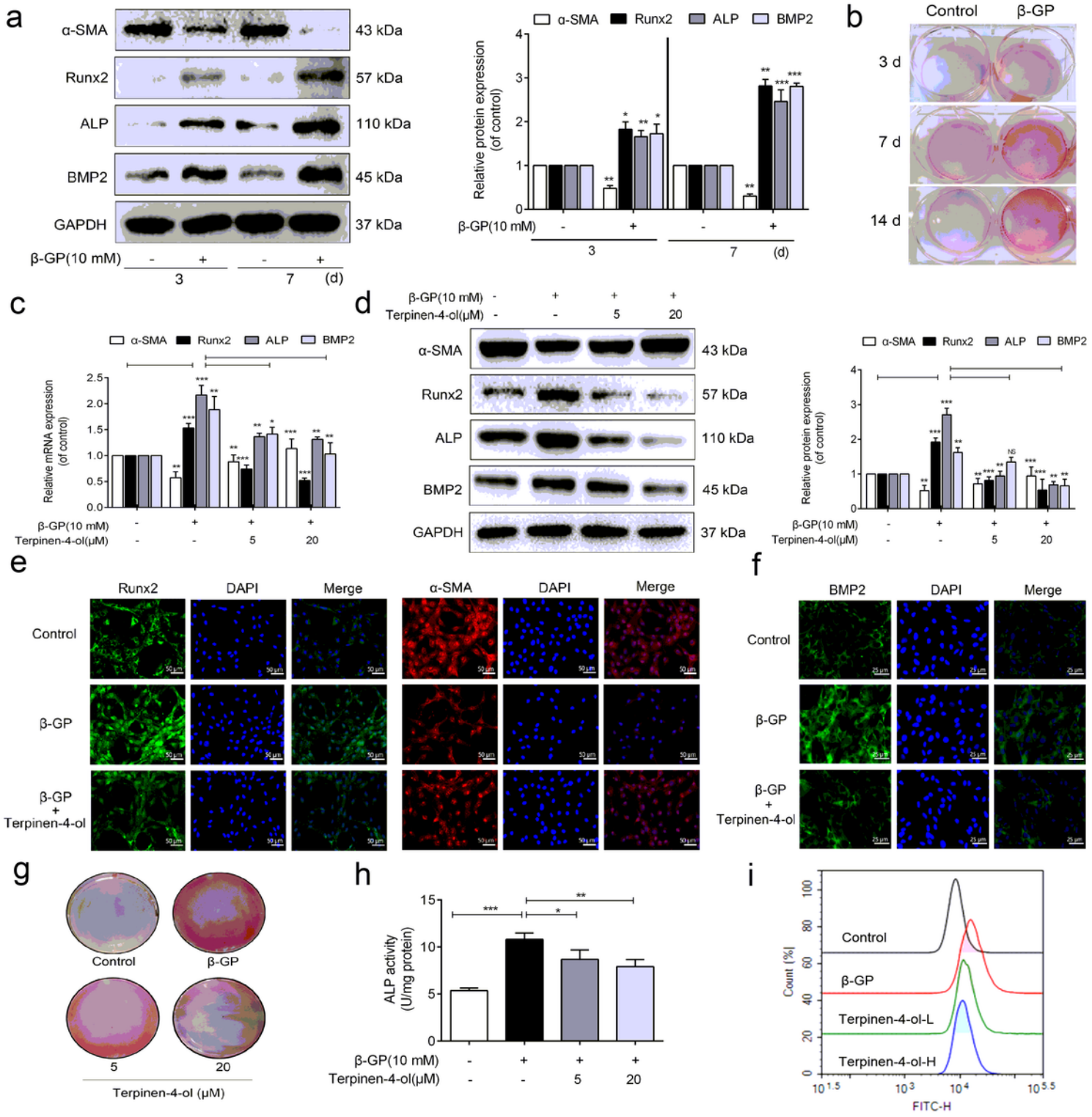

Figure 2

Terpinen-4-ol inhibits β-GP-induced calcium deposition and phenotypic switching in VSMCs. (a) Western blotting showing the levels of α-SMA, Runx2, ALP, and BMP2 in VSMCs treated with 10 mmol/L β-GP for 3 and 7 days. (b) VSMCs were cultured with 10 mmol/L β-GP for the indicated days (3, 7, and 14 days). Significant increases in mineralized nodules were detected by alizarin red staining compared with those in the control. (c) qPCR analysis of α-SMA, Runx2, ALP, and BMP2 mRNA levels in VSMCs treated with or without the indicated concentrations of terpinen-4-ol; the data were normalized to that of GAPDH. (d) Western blotting showing the expression of α-SMA, Runx2, ALP, and BMP2 in VSMCs. The data represent densitometric quantification of VC-related protein normalized to that of GAPDH. (e) Representative immunofluorescence microscopy images of Runx2 and α-SMA in VSMCs after β-GP treatment in the presence or absence of terpinen-4-ol (20 μmol/L) for 48 h. Runx2 (green fluorescence), α-SMA (red fluorescence), and cell nuclei were stained with DAPI (blue fluorescence). Magnification, ×200; scale bars, 50 μm. (f) Immunofluorescence analysis revealed the modulation of BMP2 expression in VSMCs after β-GP treatment in the presence or absence of terpinen-4-ol (20 μmol/L) for 48 h. BMP2 (green fluorescence) and cell nuclei were stained with DAPI (blue fluorescence). Magnification, ×400; scale bars, 25 μm. (g) VSMCs were cultured with or without β-GP medium in the presence or absence of terpinen-4-ol for 7 days. Alizarin red staining was performed to visualize VSMC calcium nodules. (h) ALP activity was measured using ALP kits, normalized to the cellular protein content. (i) Cells were treated with β-GP in the presence or absence of 20 μmol/L terpinen-4-ol for 7 days, and cytosolic Ca2+ levels were measured via flow cytometry using Fluo-4 AM. All data represent the mean ± SEM of more than three experiments. *P < 0.05, **P < 0.01, ***P < 0.001.

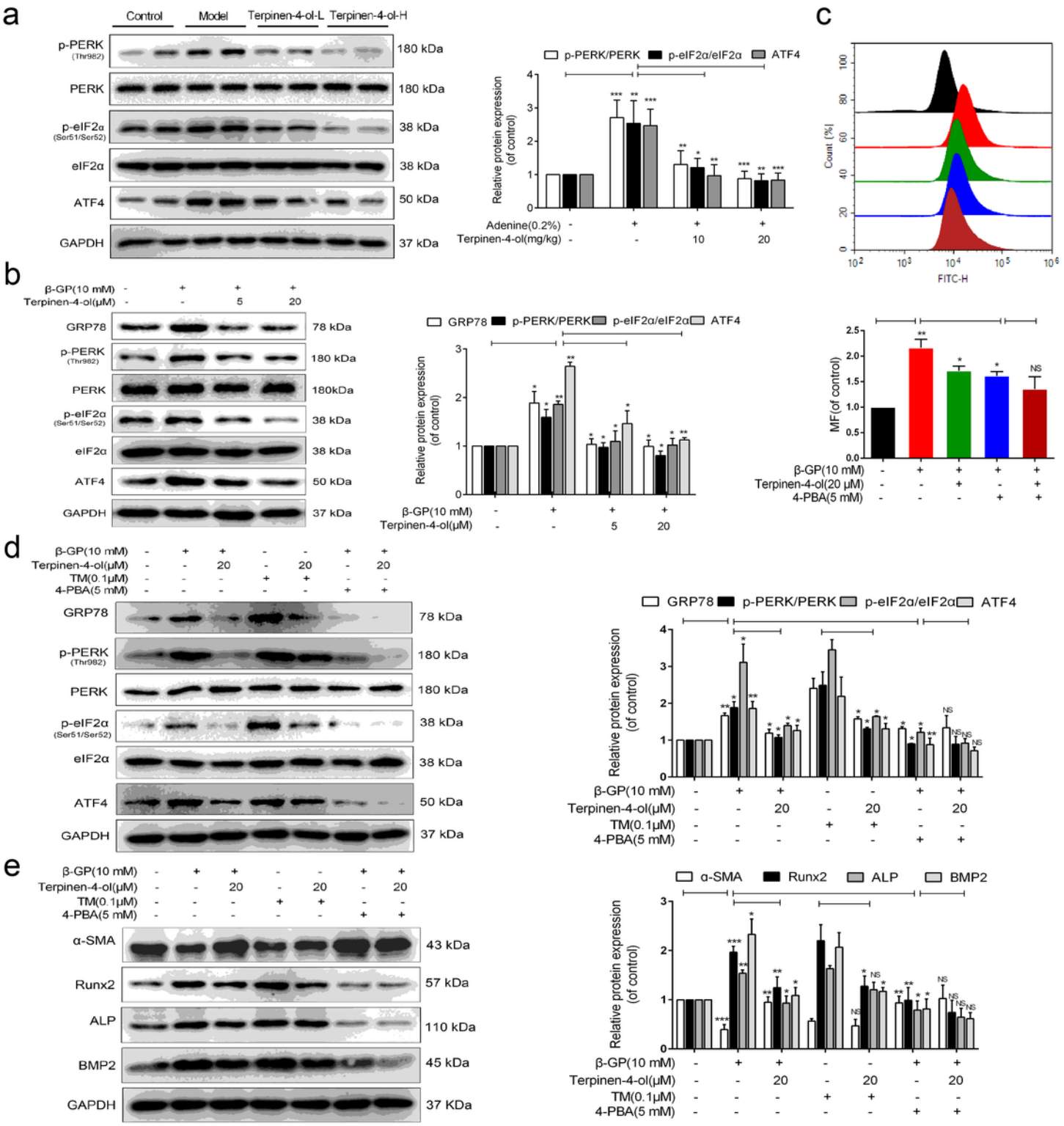

Figure 3

Terpinen-4-ol suppresses VC through inhibition of the PERK-eIF2α-ATF4 pathway in vivo and in vitro. (a) Representative western blot bands and semiquantitative analysis of ER stress markers (p-PERK, PERK, p-eIF2a, eIF2a, and ATF4) in mouse aortas. (b) Western blotting analysis of ER stress markers (GRP78, p-PERK, PERK, p-eIF2a, eIF2a, and ATF4) in VSMCs treated with or without the indicated concentrations of terpinen-4-ol; the data were normalized to that of GAPDH. (c) Cytosolic Ca2+ levels were measured via

flow cytometry using Fluo-4 AM in VSMCs treated with β-GP in the presence or absence of 20 μmol/L terpinen-4-ol for 7 days. Histogram overlays display fluorescence intensities (above) and mean fluorescence intensity (MFI, below) after treatment. (d) Respectively, terpinen-4-ol and 4-PBA attenuated β-GP- or TM-mediated ER stress markers (GRP78, p-PERK, PERK, p-eIF2a, eIF2a, and ATF4) in VSMCs. (e) Respectively, terpinen-4-ol and 4-PBA inhibited β-GP- or TM-induced changes in the levels of VC-related markers. Protein levels were normalized to GAPDH levels and presented as fold changes relative to those in control cells. All data represent the mean ± SEM of more than three experiments. NS indicates no significance. *P < 0.05, **P < 0.01, ***P < 0.001.

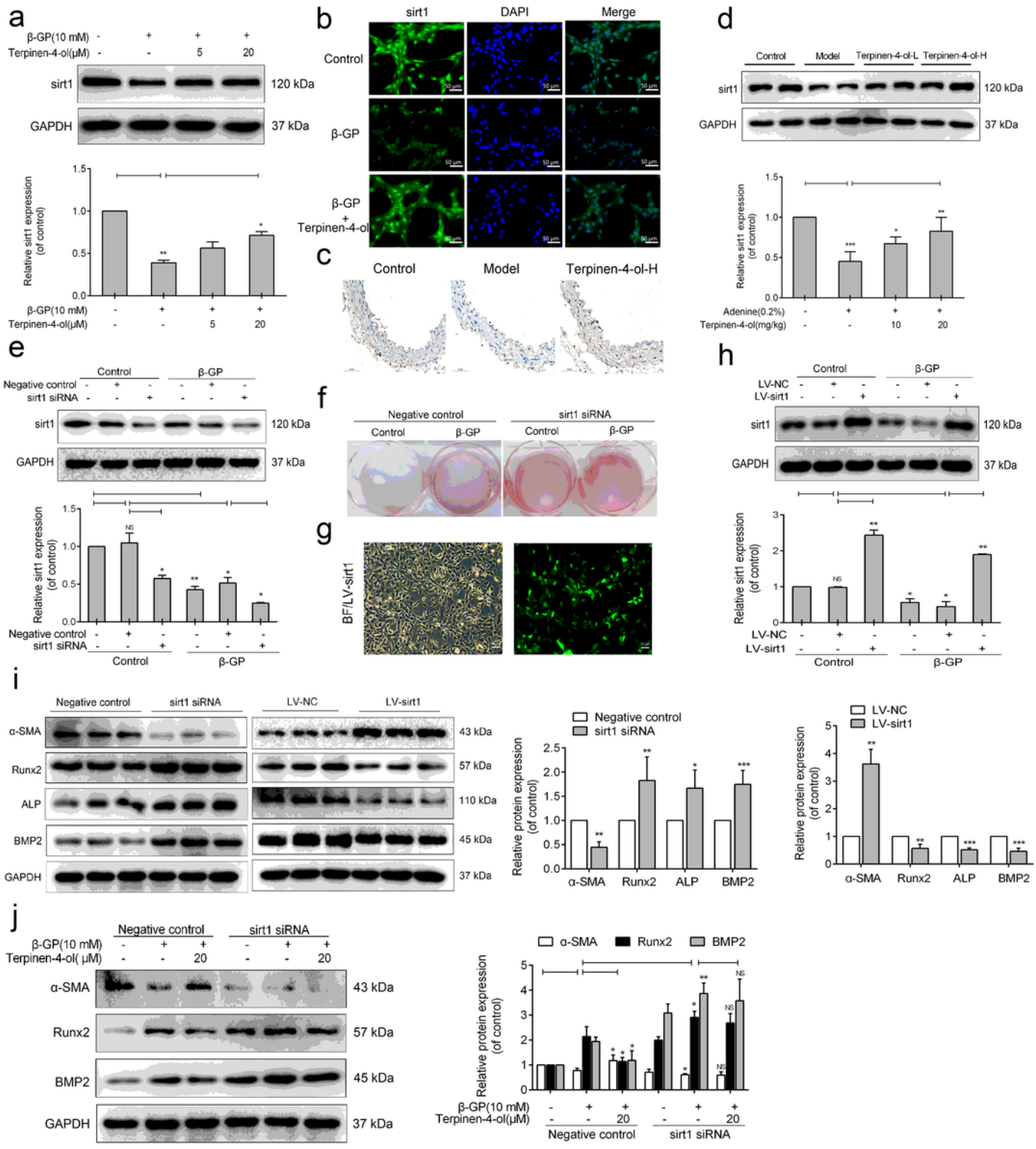

Figure 4

Terpinen-4-ol inhibits VC by upregulating sirt1. (a) VSMCs treated with or without β-GP (10 mM) were treated with terpinen-4-ol (20 μmol/L) for 7 days. Relative protein levels of sirt1 was quantified via western blotting, and the data were normalized to the levels of GAPDH. (b) Immunofluorescence analysis revealing the modulation of sirt1 expression in VSMCs after β-GP treatment with or without terpinen-4-ol (20 μmol/L) for 48 h. sirt1 (green fluorescence) and cell nuclei were stained with DAPI (blue fluorescence)

(×200; scale bars, 50 μm). (c) Representative immunofluorescence staining of sirt1 in mouse aortas. (d) Representative western blot bands of sirt1. (e) Western blotting analysis of VSMCs with silenced sirt1. The data were normalized to that of GAPDH. (f) Alizarin red staining was performed to visualize calcium nodules in VSMCs. (g) Bright-field (BF) and enhanced GFP (LV-sirt1) of sirt1 in VSMCs transfected with LV-sirt1 (scale bar: 50 μm). (h) Western blotting analysis of LV-induced overexpression of sirt1 in VSMCs. The expression of sirt1 increased in VSMCs transfected with LV-sirt1 and treated with or without β-GP for 7 days, and the data were normalized to that of GAPDH. (i) VSMCs transfected with sirt1 siRNA, negative control siRNA, LV-sirt1, or LV-NC were cultured with β-GP. Western blotting analysis results of α-SMA and osteoblastic differentiation markers (ALP, BMP2, and Runx2), normalized to the data of GAPDH (n=6). (j) VSMCs were transfected with sirt1 siRNA or negative control and then incubated with β-GP (10 mmol/L) in the presence or absence of terpinen-4-ol (20 μmol/L) for 7 days. Western blotting analysis of α-SMA and osteoblastic differentiation markers (ALP, BMP2, and Runx2), with GAPDH as a loading control. All data represent the mean ± SEM of more than three experiments. NS indicates no significance. *P < 0.05, **P < 0.01, ***P < 0.001.

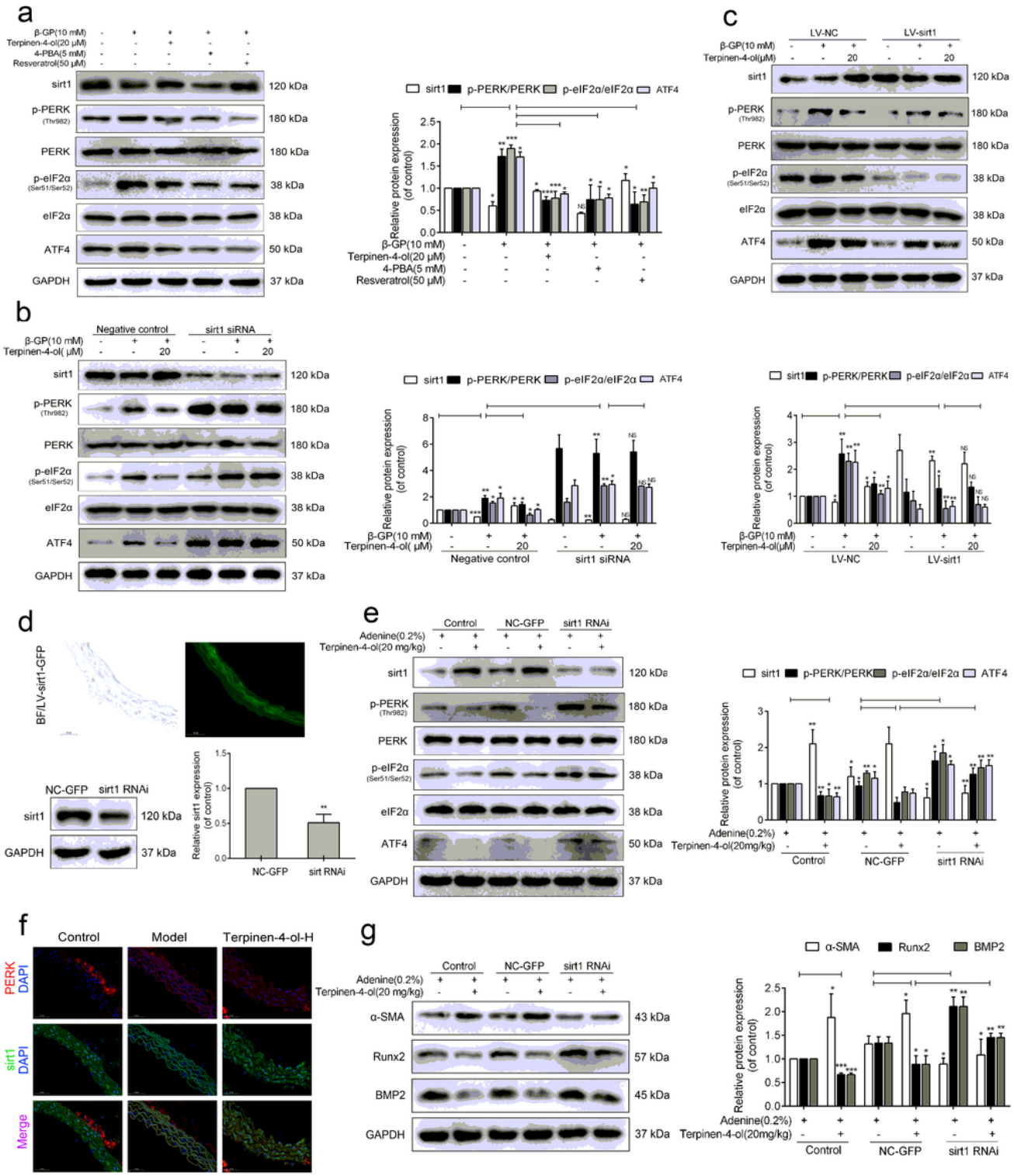

Figure 5

Terpinen-4-ol alleviates β-GP-induced ER stress in a sirt1-dependent manner. (a) VSMCs treated with or without β-GP (10 mM) were treated with terpinen-4-ol (20 μmol/L), the sirt1 agonist resveratrol (50 μmol/L), and the ER stress inhibitor 4-PBA (5 mmol/L) for 7 days. Western blotting analysis of sirt1 and ER stress markers (p-PERK, PERK, p-eIF2a, eIF2a, and ATF4) was performed in VSMCs, and GAPDH was used as a loading control. (b) Western blotting results of sirt1 and ER stress markers (p-PERK, PERK, p-

eIF2a, eIF2a, and ATF4) in VSMCs, with GAPDH as a loading control. VSMCs were transfected with sirt1 siRNA or negative control and then incubated with β-GP (10 mmol/L) in the presence or absence of terpinen-4-ol (20 μmol/L) for 7 days. (c) Western blotting analysis results of sirt1 and ER stress markers (p-PERK, PERK, p-eIF2a, eIF2a, and ATF4) in VSMCs, with GAPDH used as a loading control. VSMCs were transfected with LV-sirt1 or LV-NC and then incubated with β-GP (10 mmol/L) in the presence or absence of terpinen-4-ol (20 μmol/L) for 7 days. (d) Enhanced GFP and western blot band of sirt1 in LV-transfected mouse aortas (scale bar: 50 μm). (e) Western blotting analysis of ER stress markers (p-PERK, PERK, p-eIF2a, eIF2a, and ATF4) in LV-sirt1 RNAi-transfected mouse aortas, with GAPDH as a loading control. (f) PERK expression in the aortas was determined by immunofluorescent staining of aortic root cross-sections and quantitative analysis of the fluorescent intensity (scale bar: 50 μm). (g) Western blotting analysis of α-SMA, BMP2, and Runx2 in LV-sirt1 RNAi-transfected mouse aortas, with GAPDH as a loading control. All data represent the mean ± SEM of more than three independent experiments. NS indicates no significance. *P < 0.05, **P < 0.01, ***P < 0.001.

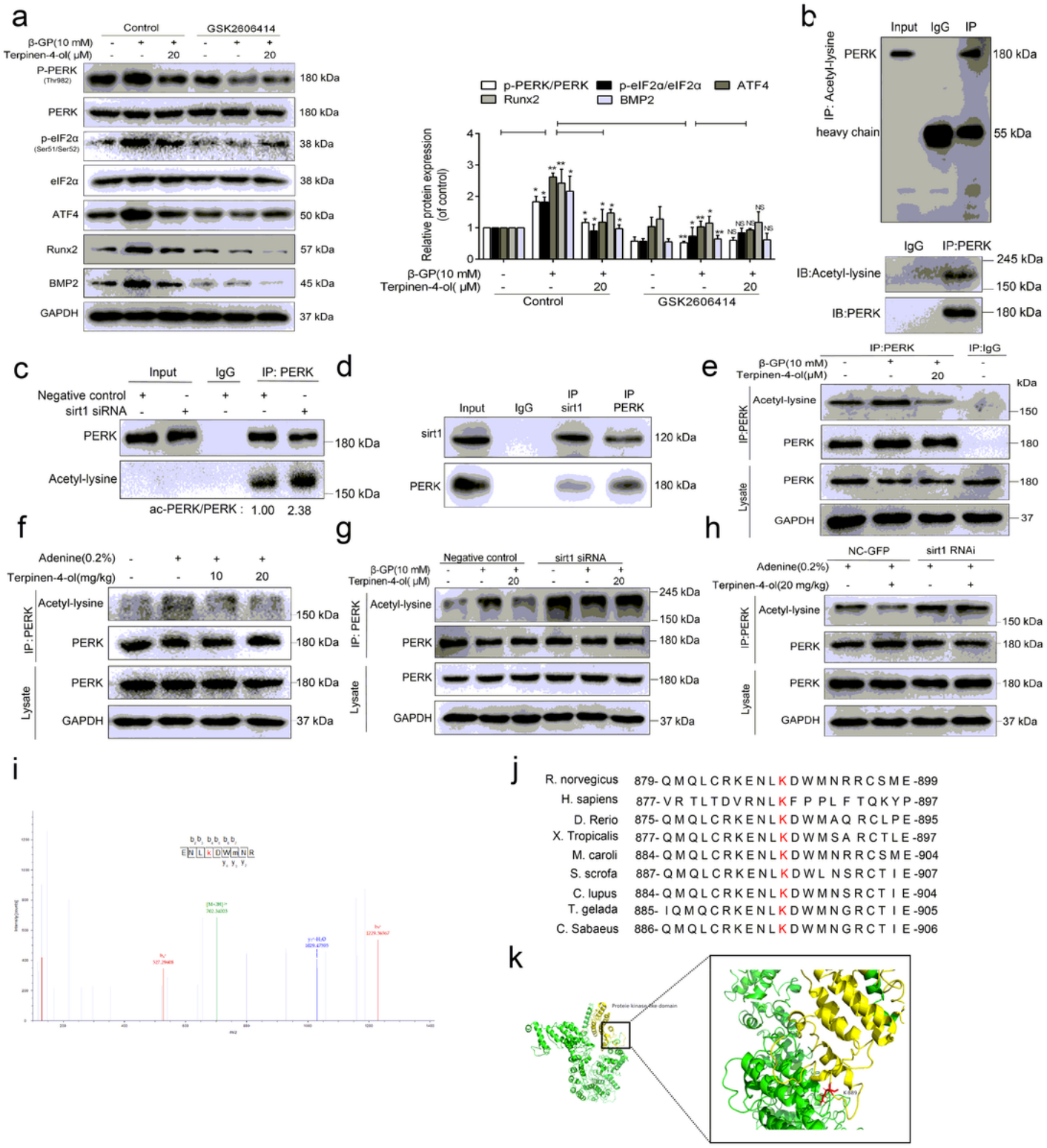

Figure 6

Terpinen-4-ol improves ER stress-induced VC through sirt1-mediated PERK deacetylation. (a) VSMCs treated with or without β-GP (10 mmol/L) were treated with terpinen-4-ol (20 μmol/L) or the PERK inhibitor GSK2606414 (5 μmol/L) for 7 days. Western blotting analysis of p-PERK, PERK, p-eIF2a, eIF2a, ATF4, BMP2, and Runx2 was performed in VSMCs, and GAPDH was used as a loading control. (b) PERK was immunoprecipitated from VSMC lysates, and its acetylation was analyzed by immunoblotting with

an anti-acetyl-lysine antibody. Immunoprecipitation of acetylated proteins from VSMC lysates was followed by immunoblotting with the indicated antibodies; Input: supernatant before immunoprecipitation; IP: immunoprecipitate; IgG: negative control. (c) VSMCs were transfected with sirt1 siRNA or negative control, PERK was immunoprecipitated, and its level of acetylation was determined by immunoblotting with an anti-acetyl-lysine antibody. Ratios of acetylated versus total PERK are presented. (d) Physical interaction between endogenous sirt1 and PERK was shown by co-immunoprecipitation. sirt1 was precipitated from VSMC lysates with anti-sirt1 antibody and blotted with anti-PERK antibody, and vice versa. (e) Immunoprecipitation of acetylated proteins from VSMC lysates was followed by immunoblotting with the indicated antibodies. Input: supernatant before immunoprecipitation, IgG: negative control, rabbit IgG; IP: immunoprecipitated. (f) Acetylated lysine and total PERK expression in the aortas of C57BL/6J mice as described in Figure 1 by immunoprecipitation and western blotting analysis. (g) Immunoprecipitation of acetylated proteins from VSMC lysates was followed by immunoblotting with the anti-PERK antibody. Input: Supernatant before immunoprecipitation. (h) Acetylated lysine and total PERK expression in the aortas, as analyzed by immunoprecipitation and western blotting analysis. (i) Schematic representation of the mass spectrometry results of PERK in VSMCs. PERK was purified by immunoprecipitation with Protein A/G PLUS. The immunoprecipitated PERK was subjected to SDS-PAGE, and the band corresponding to PERK was digested in gel with trypsin. The labeled peptides were analyzed by LC-MS/MS. (j) Sequence alignment of the region surrounding the K889 residues of PERK. (k) The 3D crystal structure of PERK shows that K889 (red) is located in the protein kinase-like domain (yellow).

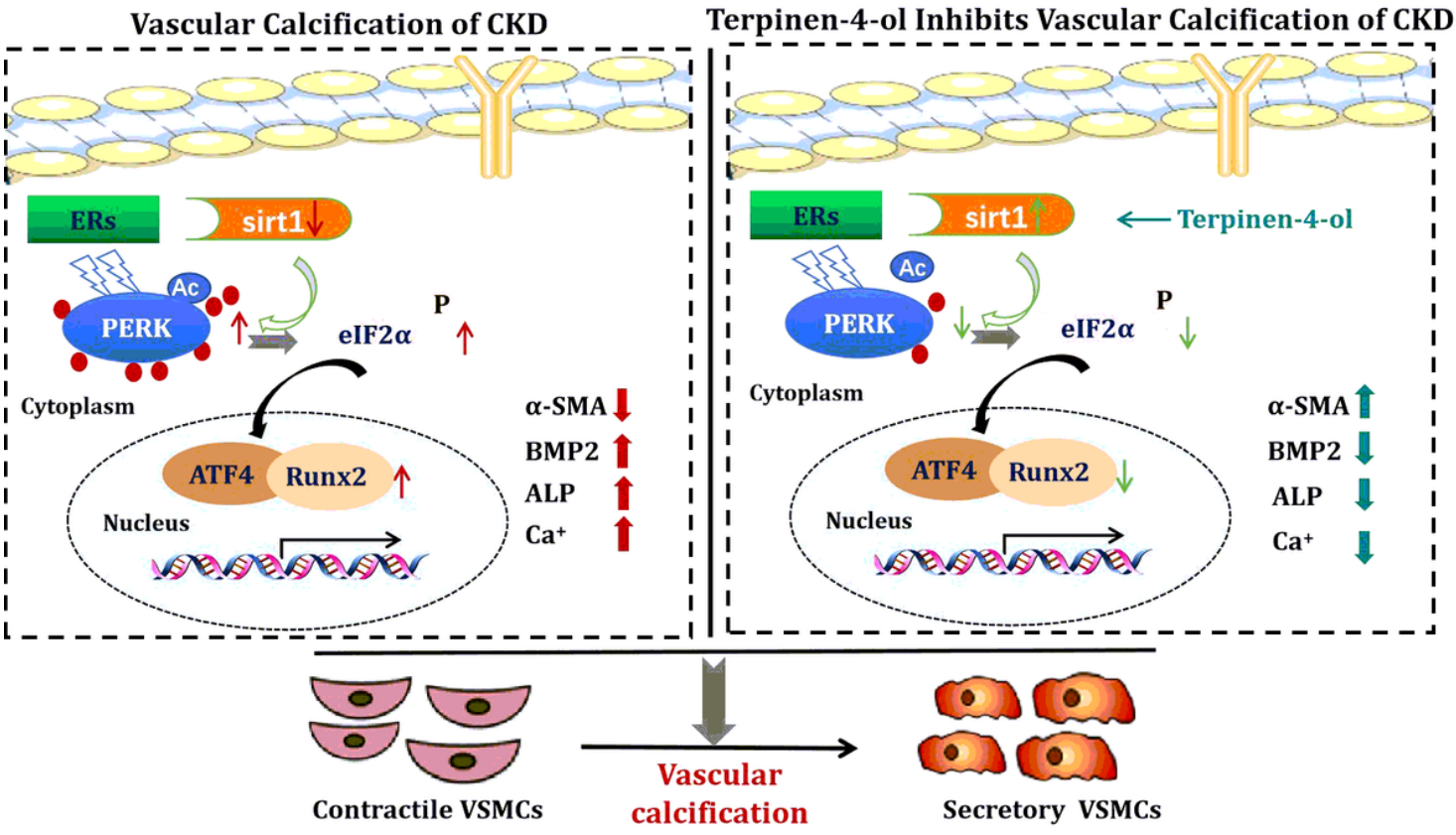

Figure 7

A schematic diagram depicting the possible mechanism underlying the inhibitory effects of terpinen-4-ol on ER stress-induced VC.

Supplementary Files

This is a list of supplementary files associated with this preprint. Click to download.

- SupportingInformationfor.docx